



Sulfur dioxide exploitation by electrochemical oxidation of sulfite in near-neutral pH electrolytes: A kinetics and mechanistic study

R.A. Márquez-Montes^a, R.E. Orozco-Mena^a, D. Lardizábal-Gutiérrez^b, D. Chávez-Flores^a, A. López-Ortíz^b, V.H. Ramos-Sánchez^{a,*}

^a Cuerpo Académico de Química Aplicada y Educativa, Facultad de Ciencias Químicas, Universidad Autónoma de Chihuahua, Nuevo Campus Universitario, Circuito Universitario, Chihuahua Chih., C.P. 31125, Mexico

^b Centro de Investigación en Materiales Avanzados, S.C., Miguel de Cervantes #120, Complejo Industrial Chihuahua, Chih., C.P. 31136, Mexico



ARTICLE INFO

Keywords:
Sulfite electrooxidation
Kinetics
Palladium
Reaction mechanism

ABSTRACT

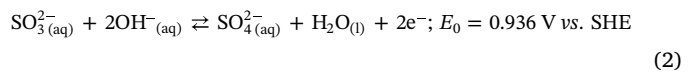
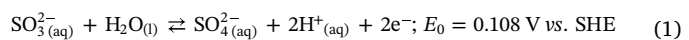
Electrochemical oxidation of sulfite ions offers an efficient and profitable approach to the conversion of sulfur dioxide, a harmful air pollutant, into valuable by-products *via* flue gas desulfurization. Here, the electrochemical oxidation of sulfite in near-neutral pH electrolytes is studied in order to determine kinetic parameters and a reaction mechanism. Sulfite electrooxidation on palladium is demonstrated at pH 7.5 and 8.5, the latter being comparable to platinum. Anodic charge transfer coefficients and non-linear reaction orders are linked to a mechanism which involves sulfite adsorption at low potentials. This study proves that sulfite electrooxidation on palladium at near-neutral pH is a useful approach for sulfur dioxide exploitation.

1. Introduction

Air pollution is assessed by the air quality index, which is based on measurements of particulate matter, O₃, NO₂, CO and SO₂. In the case of the latter, the World Health Organization has established 20 µg/m³ as a feasible goal for low- and middle-income countries to protect public health, otherwise deaths caused by air pollution are expected to increase [1,2]. Countries with large industries based on fossil fuels, like China, make a significant contribution to global SO₂ emissions, causing serious health and environmental issues [3]. The most effective method to control SO₂ emissions is flue gas desulfurization (FGD), in which SO₂ is scrubbed and then chemically absorbed into sulfite (SO₃²⁻) at a slightly alkaline pH [4]. It is noteworthy that ammonia-based FGD yields (NH₄)₂SO₄, a potential fertilizer, as a by-product, thus improving the economic feasibility of SO₂ capture [5]. Oxidation treatments based on O₃ are often employed [6]. However, sulfite oxidation can also produce additional benefits such as the generation of an energy vector: hydrogen [7].

A small number of sulfur-based thermochemical cycles for hydrogen production depend on the electrochemical oxidation of S(IV) species [8]. In acidic media SO₂ electrolysis in the hybrid sulfur cycle (HyS) has been studied, while in slightly alkaline media the electrooxidation of ammonium sulfite within the sulfur-ammonia (SA) cycle has been explored [9]. However, sulfite electrooxidation proceeds in both acidic

and alkaline media, as shown in Eq. (1) and Eq. (2), respectively [10]:



Hydrogen evolution in the latter has been investigated previously [9]. However, there is a lack of experimental kinetic data. Further sulfite electrooxidation applications at high pH have been extensively investigated, ranging from developing analytical methods for the wine industry [11] to studying kinetics in applications such as oxygen scavenging [12], wastewater treatment [13], electroplating [14], and sensors [15]. Typically, platinum [12] and gold [14] electrodes have been used because of their good catalytic activity [16]. Palladium offers an alternative due to its similar catalytic behavior [17,18].

However, kinetic data is still required to understand sulfite electrooxidation over palladium, as it has been shown that the reaction mechanism in noble metals is highly dependent on surface composition and pH [19,20]. Therefore, we aim to define kinetic parameters and the reaction mechanism of sulfite electrooxidation at a near-neutral pH using a Pd/C electrode. This will provide the data necessary to improve the removal of SO₂, a harmful pollutant, in an approach based on ammonia FGD which leads to valuable by-products, *i.e.*, a fertilizer (ammonium sulfate) and an energy vector (hydrogen).

* Corresponding author.

E-mail address: vramos@uach.mx (V.H. Ramos-Sánchez).

2. Experimental

All solutions were prepared using deionized water and analytical grade reagents, 94.6% pure or better: Na₂SO₃ (Alfa Aesar®), Na₂SO₄ (Alfa Aesar®), (NH₄)₂SO₃ (Alfa Aesar®), (NH₄)₂SO₄ (Alfa Aesar®), KH₂PO₄ (Sigma-Aldrich®), and Na₂HPO₄ (Sigma-Aldrich®). Fresh sulfite solutions with concentrations ranging from 25 to 60 mM were prepared using a 0.5 M sulfate solution as solvent, and the pH was adjusted (7.5 for ammonium and 8.5 for sodium) by means of a 10 mM phosphate buffer.

A three-electrode configuration in a jacketed cell (Gamry®) was used: as working electrode, a glassy carbon disc in a Teflon cylinder (Pine Instruments®) with a geometric area of 0.196 cm² was used as the substrate for Pd/C electrocatalysts; a Pt foil ($A = 2 \text{ cm}^2$, Aldrich) was used as the counter electrode; and a saturated calomel electrode (SCE) was used as the reference electrode.

High-quality electrocatalyst films were prepared as described previously [21,22]. A catalytic ink was prepared by dispersing a suitable amount of Pd/C (Aldrich®, 10 wt% loading) in a water/isopropanol/ionomer mixture. A FAA-3 hydroxyl anion exchange ionomer (FuMA-Tech, 10 wt% in *N*-methyl-2-pyrrolidone) was used to improve the adhesion of the catalytic film, as well as to favor hydroxyl transport. The initial Pd loading was estimated to be 20.4 µg cm⁻². The loading figures were rectified after polarization experiments by quantifying the Pd concentration in the previously used supporting electrolyte by means of total reflection X-ray fluorescence.

Electrochemical measurements were carried out in an Interface 1000 potentiostat/galvanostat (Gamry®). The cell temperature was set by means of a water jacket on a hot plate. The temperature was stable within ± 0.5 °C. Before each measurement, the cell was filled with 150 mL of a control electrolyte (*i.e.*, supporting electrolyte and buffer). The Pd-coated glassy carbon electrode (GCE) was soaked in deionized water, attached to the shaft of the rotator (Pine Instruments MSR), and immersed in the control electrolyte. The working electrode was electrochemically cleaned by cyclic voltammetry (CV) between -0.85 and 0.15 V vs. SCE for 30 cycles at 100 mV s⁻¹, until stabilization occurred. Afterwards, the control electrolyte was replaced with 150 mL of fresh electrolyte containing the desired sulfite concentration. CVs were recorded between -0.85 and 1.20 V vs. SCE at 50 mV s⁻¹. The background currents from the control electrolyte were subtracted to eliminate contributions from the capacitive current and water electrooxidation. Ohmic drop was compensated using the current interruption technique.

3. Results and discussion

3.1. Sulfite polarization curves

Polarization measurements on a stationary Pd-coated GCE were performed as CV sweeps from -0.85 to 1.20 V with two electrolytes: Na₂SO₃/Na₂SO₄ and (NH₄)₂SO₃/(NH₄)₂SO₄, in order to identify the processes occurring on Pd. The resulting voltammograms are shown in Fig. 1. The cathodic sweeps only exhibit reduction peaks between -0.40 and -0.85 V. The peak around -0.55 V (1C) is associated with the reduction of palladium (II) oxide [23,24], while peak 2C is explained by hydrogen adsorption [25]. No other remarkable reduction peaks are observed, suggesting that sulfite electrooxidation is irreversible within the studied potential range, which is in agreement with previous studies [12,13]. Anodic sweeps show a peak at *ca.* -0.35 V (1A), which is attributed to the formation of palladium (II) oxide (*via* OH⁻ adsorption) and hydrogen desorption [23,26]. A current increase associated with sulfite oxidation starts at *ca.* 0.08 V, with a maximum around 0.75 V (2A). Note that the peak current in sodium sulfite electrooxidation (Fig. 1b) at 100 mV s⁻¹ is comparable to that observed for Pt (*ca.* 7 mA cm⁻²) [12]. Finally, a water oxidation peak is seen beyond 1.0 V.

Fig. 2 shows the effect of rotation rate and sulfite concentration on Pd-coated GCEs for both electrolytes. Fresh catalyst layers are used exclusively in the latter. Both onset potentials start at *ca.* 0.08 V. To ease the discussion of Fig. 2a and Fig. 2b, these have been divided into three regions, based on their rotation rate dependence [27]. First, a kinetics-controlled region from 0.08 to 0.40 V, in which the current is defined by the charge transfer on the electrode (1). Then, a mixed control region from 0.40 to 0.90 V, in which both charge and mass transfer have important effects (2). Finally, a mass transfer-limited region from 0.90 to 1.20 V, in which the electrooxidation rate depends on how fast electroactive species reach the electrode (3). Note that, as shown in Fig. 1, sodium sulfite exhibits the highest limiting currents. Furthermore, to ensure that this behavior is due to the electrocatalytic activity of Pd, a CV from a bare GCE is included in the supplementary data (p. S2).

The results outlined above lead to the following insights:

- Since the limiting current density is linearly dependent on the square root of the rotation rate in both sulfites, it is feasible to estimate effective diffusion coefficients using the Levich equation [27]:

$$j_L = 0.62nFD^{2/3}\nu^{-1/6}c_b\omega^{1/2} \quad (3)$$

where j_L is the limiting current density, n is the number of electrons transferred, F is Faraday's constant, D is the diffusion coefficient, ν is the kinematic viscosity, c_b is the bulk concentration of sulfite, and ω is the angular rotation rate.

- Ammonium sulfite is affected by kinetics, whereas sodium sulfite is solely controlled by diffusion. This is based on the intercept shift (inset of Fig. 2a, *ca.* 9 A m⁻²) [28].
- The rate-determining step (rds) involves sulfite ions, since the current density is dependent on sulfite concentration in both scenarios [13].

3.2. Determination of kinetic parameters

The potential-current curves from Fig. 2 are used to obtain kinetic parameters. Numerical optimization of the data is described in the following sections.

3.2.1. Anodic charge transfer coefficient

The anodic charge transfer coefficient (β) is related to the electron transfer. Hence, it is used to evaluate kinetics and reaction mechanisms [27]. β can be estimated using data from both kinetics and mixed control regions by the Nernst diffusion layer approach [12]:

$$\log\left(\frac{j}{1-j/j_L}\right) = \frac{\beta nF}{2.303RT}E + \text{const} \quad (4)$$

where j is the current density, R is the gas constant, T is the absolute temperature, and E is the electrode potential. The slope of the fitted curve using Eq. (4) represents the Tafel slope, since $j/(1-j/j_L)$ is equal to the kinetic current density j_k . Fitted curves at different rotation rates from Fig. 2a and Fig. 2b are shown in Fig. 3. Tafel slopes and the corresponding values of β (22 °C, $n = 1$) are given in Table 1. The Tafel slopes at low potentials are similar in both electrolytes. Near 0.28 V, both Tafel slopes increase. Note: Pt exhibits similar behavior *ca.* 0.62 V [12].

3.2.2. Electrochemical reaction order

The reaction order relates to the variation of current density with the concentration of the *i*-th species at a constant potential, as shown in Eq. (5) [13]:

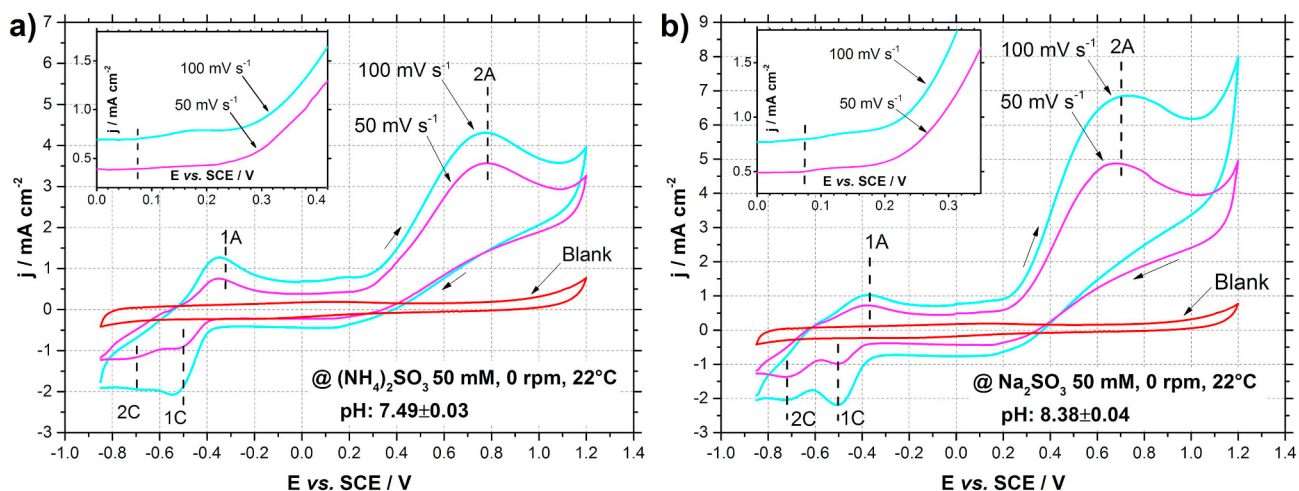


Fig. 1. CVs on a stationary, Pd-coated GCE in (a) ammonium and (b) sodium electrolytes. Insets display a close-up for better visualization of the onset potential.

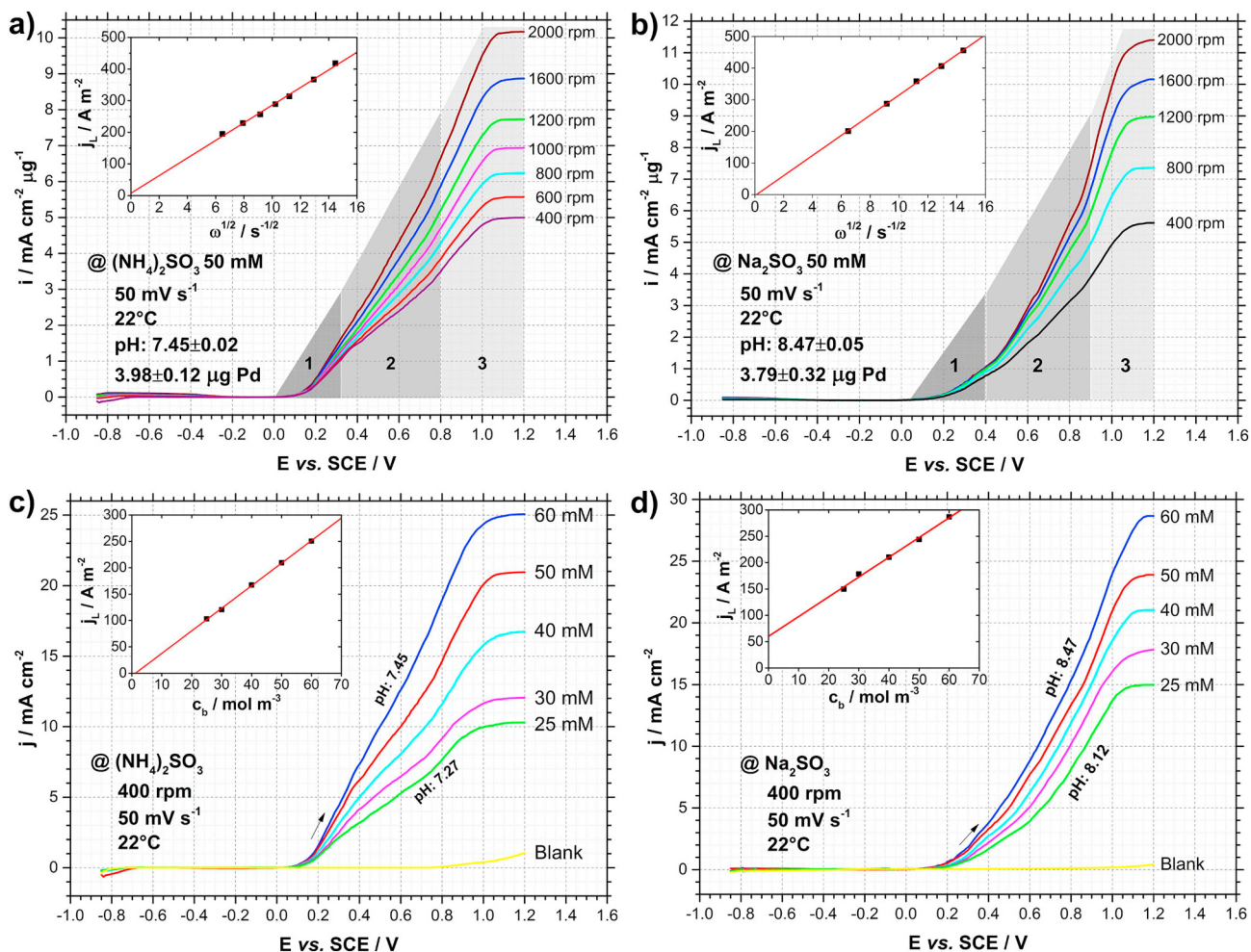


Fig. 2. Potential–current curves of ammonium (left) and sodium (right) sulfite electrooxidation at different rotation rates (above) and sulfite concentrations (below). Insets show the dependence of j_L on $\omega^{1/2}$ and c_b . Note: Fig. 2a and Fig. 2b are expressed in terms of electrocatalyst mass.

$$n_i = \left(\frac{\partial \log j}{\partial \log c_i} \right)_E \quad (5)$$

where n_i is the reaction order of species i . To obtain n_i , the concentration of only one reactant must be varied, giving the reaction order with respect to that component. In this study, pH control ensures constant concentration of protons/hydroxide ions. Moreover, earlier studies

have concluded that the reaction order with respect to hydroxide ions is zero [13]. Hence, Eq. (6) is used in the kinetics-controlled region of Fig. 2c and Fig. 2d [12]:

$$\log j = n_i \log c_b + \text{const} \quad (6)$$

The resulting plots are shown in Fig. 4, the slopes providing the reaction order with respect to sulfite.

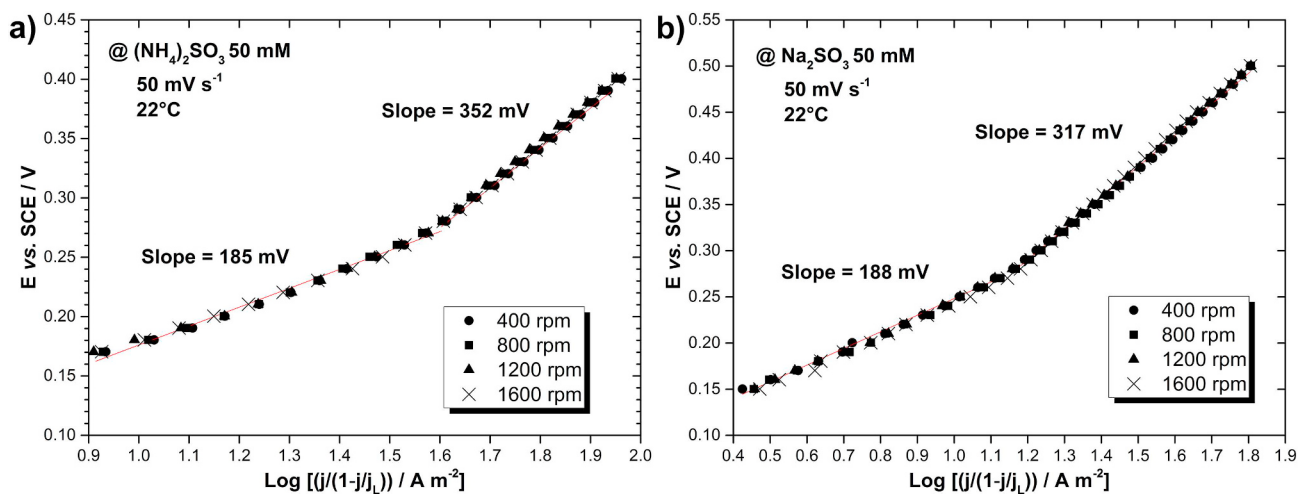


Fig. 3. Potential as a function of $\log(j/(1 - j/j_L))$ in (a) ammonium and (b) sodium electrolytes.

Table 1
Tafel slopes (mV) and anodic charge transfer coefficients.

$(\text{NH}_4)_2\text{SO}_3$	Tafel slope	β	Na_2SO_3	Tafel slope	β
0.15 to 0.28 V	185.5	0.32	0.15 to 0.27 V	188.1	0.31
0.28 to 0.45 V	352.3	0.18	0.27 to 0.50 V	317.4	0.19

The behaviour described above leads to the following insights:

- Sulfite electrooxidation in both electrolytes is controlled by the same electron transfer at low potentials (0.15 to 0.28 V), as shown by comparable values of β .
- Both Pt and Pd exhibit similar reaction mechanisms, since the Tafel slopes for Pd in the low potential region are close to those found for Pt [12].
- A subtle difference in β is evident in both electrolytes at high potentials (0.27–0.50 V), which makes it difficult to compare sodium and ammonium electrolytes. Only β for sodium sulfite resembles that for Pt [12].

In the mixed control region, a steady-state condition occurs in which the heterogeneous reaction rate is equal to the diffusion rate. Expressions for the heterogeneous reaction rate and diffusion rate in terms of the current density are shown in Eq. (7) and Eq. (8), respectively:

$$j = nFk_s c_s^{n_i} \quad (7)$$

$$j = nFD \left(\frac{c_b - c_s}{\delta} \right) = j_L \left(1 - \frac{c_s}{c_b} \right) \quad (8)$$

where k_s is the general heterogeneous rate constant, c_s is the surface concentration, δ is the diffusion layer thickness, and $j_L = nFDc_b/\delta$. By combination of Eq. (7) and Eq. (8), n_i is obtained in the mixed control region using Eq. (9) [12]:

$$\log j = n_i \log \left(1 - \frac{j}{j_L} \right) + \log j_k \quad (9)$$

Fig. 5 shows plots of Eq. (9) using data from Fig. 2. The insets display Tafel slopes resulting from the intercepts (*i.e.*, $\log j_k$), which allow determination of β .

At low potentials (Fig. 4) the reaction order with respect to sulfite is almost 1, while at higher potentials (Fig. 5), the reaction order progressively increases up to 1.9 in both electrolytes. The values of β from the Tafel slopes (0.18 for ammonium and 0.20 for sodium) agree with those in Table 1 at high potentials. Fractional orders suggest that sulfite adsorption proceeds in both electrolytes; as also occurs with Pt [12].

3.2.3. Temperature dependence

The dependence of the onset potential, β , and diffusion coefficients on temperature is investigated in the temperature range from 22 °C to 50 °C. Additional plots are included in the supplementary data (p. S3–S4). Table 2 shows the dependence of the onset potential on

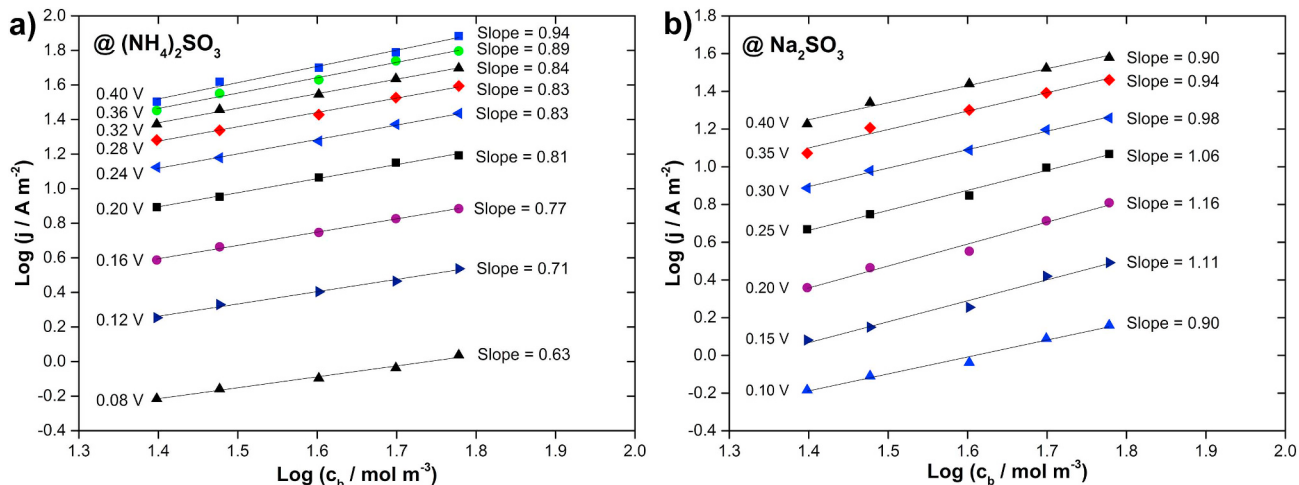


Fig. 4. $\log j$ against $\log c_b$ at different potentials in (a) ammonium and (b) sodium electrolytes.

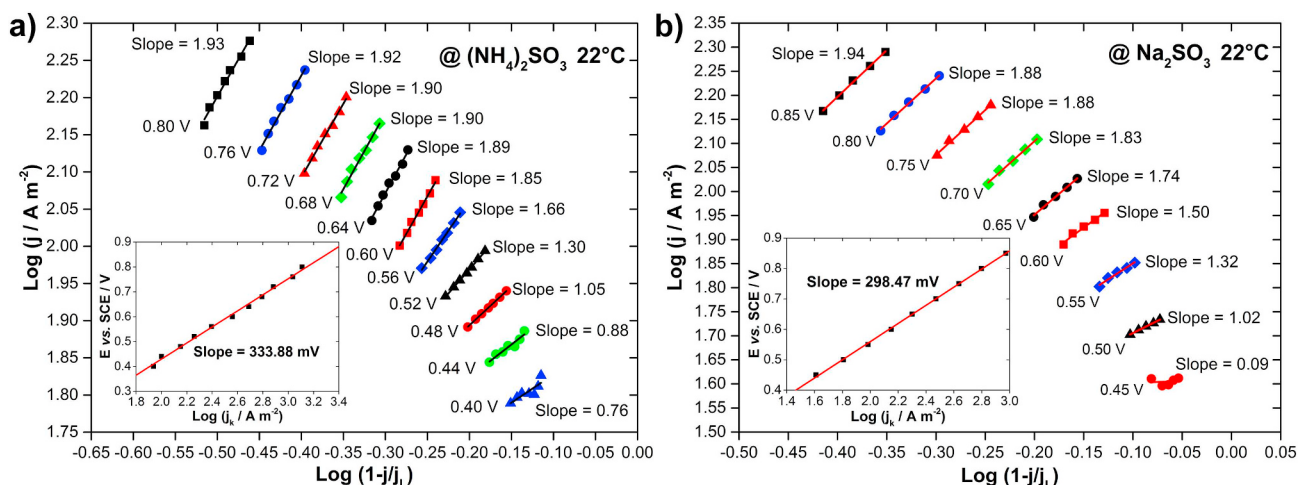


Fig. 5. $\log(j)$ as a function of $\log(1 - j/j_L)$ in (a) ammonium and (b) sodium electrolytes.

Table 2

Onset potentials (V vs. SCE) at different temperatures for both electrolytes.

T (°C)					
	22	35	40	45	50
$(\text{NH}_4)_2\text{SO}_3$	0.08	0.06	0.04	0.03	0.01
Na_2SO_3	0.07	0.06	0.05	0.03	0.01

temperature. Electrooxidation starts at lower potentials when the temperature is increased. Both electrolytes exhibit the same behavior. The onset potentials are lower than those reported for a Pt disc (0.38 V at 22 °C) [12] and graphite (0.16 to 0.04 V between 25 and 60 °C) [13]. This confirms that Pd improves electrooxidation compared to such materials.

The dependence of β on temperature is shown in Table 3. β decreases as the temperature is increased in both electrolytes, especially in the low-potential region. In the mixed control region, a very slight decrease is observed. This suggests that temperature modifies the reaction mechanism at low potentials only.

The activation energy of sulfite electrooxidation is investigated using the formal activation energy, Ω , which is applicable for kinetics of irreversible electrochemical reactions at a constant potential [29]. A detailed description is given in the supplementary data (pp. S5–S7).

The kinetic current density is used to obtain Ω , as shown in Eq. (10).

$$\log(j_k) = -\frac{\Omega}{2.303R} \left(\frac{1}{T} \right) + \text{const} \quad (10)$$

Intercepts from Eq. (9) at different temperatures are used in Eq. (10) to calculate Ω in the mixed-control region, while values of $\log(j/(1 - j/j_L))$ are used in the kinetics-controlled region. The diffusional mass transfer activation energy Z_D is obtained as follows [30]:

$$\log(D) = -\frac{Z_D}{2.303R} \left(\frac{1}{T} \right) + \text{const} \quad (11)$$

Eq. (3) is used to obtain diffusion coefficients at each temperature

Table 3

Anodic charge transfer coefficients at different temperatures (°C).

	22	35	40	45	50
$(\text{NH}_4)_2\text{SO}_3$					
Kinetics-controlled region	0.32	0.26	0.25	0.24	0.24
Mixed control region	0.18	0.17	0.16	0.16	0.16
Na_2SO_3					
Kinetics-controlled region	0.31	0.26	0.25	0.24	0.24
Mixed control region	0.19	0.19	0.18	0.18	0.18

from plots of j_L against $\omega^{1/2}$.

While Ω varies with potential, only one value of Z_D is obtained from different rotation rates. Fig. 6a and Fig. 6b show the plots of $\log(j_k)$ against T^{-1} at different potentials. The slopes give the formal activation energies. The insets describe the variation of Ω with E . Fig. 6c and Fig. 6d show plots of j_L against $\omega^{1/2}$. The insets describe $\log(D)$ as a function of T^{-1} . Values of Z_D are obtained from the slopes.

The values closely agree with previous reports on graphite (85–45 kJ mol⁻¹) [13]. Note that Ω quickly decreases in both scenarios at low potentials. Two scenarios appear above 0.40 V: a linear increment occurs for sodium sulfite, while erratic behavior is evident for ammonium sulfite. The latter limits the use of kinetic data to predict a reliable mechanism. Even so, the former scenario suggests a change in the mechanism for sodium sulfite, as reported elsewhere [13].

Both electrolytes exhibit similar diffusion processes independently of the pH, and the values of D are in good agreement with the literature: $6\text{--}12 \times 10^{-10} \text{ m}^2 \text{s}^{-1}$ in graphite [13,31] and $7.2 \times 10^{-10} \text{ m}^2 \text{s}^{-1}$ in gold [32]. Slight deviations of the effective diffusivity, especially in ammonium, are attributed to changes in the local pH within the diffusion layer [33]. The diffusional mass transfer activation energies are close to 18 kJ mol⁻¹, which indeed is the value reported by Lu et al. [13]. Thus, it can be asserted that the mass transfer of sulfite is independent of pH [14,19,20,32].

3.3. Sulfite electrooxidation mechanism

Electrooxidation of S(IV) species is complex due to pH speciation, which affects reaction mechanisms [8]. To support our proposed mechanism, sulfite electrooxidation pathways are described in the supplementary data (pp. S8–S11).

Using the results of Section 3.2, we can propose a valid mechanism based on the following insights:

- A change in the reaction mechanism is evident for both electrolytes around 0.28 V.
- The mechanism is the same at low potentials for both electrolytes despite different pH values; an increase in temperature affects both systems in the same manner.
- The mechanism for sodium sulfite closely follows that reported for Pt [12]. This is not the case for ammonium sulfite at high potentials.
- At high potentials, the mechanism is not changed by temperature. Variations of β in ammonium sulfite do not provide sufficient evidence of a different mechanism.

Based on the above points, the following mechanism is considered to best explain the behavior at low potentials in both electrolytes:

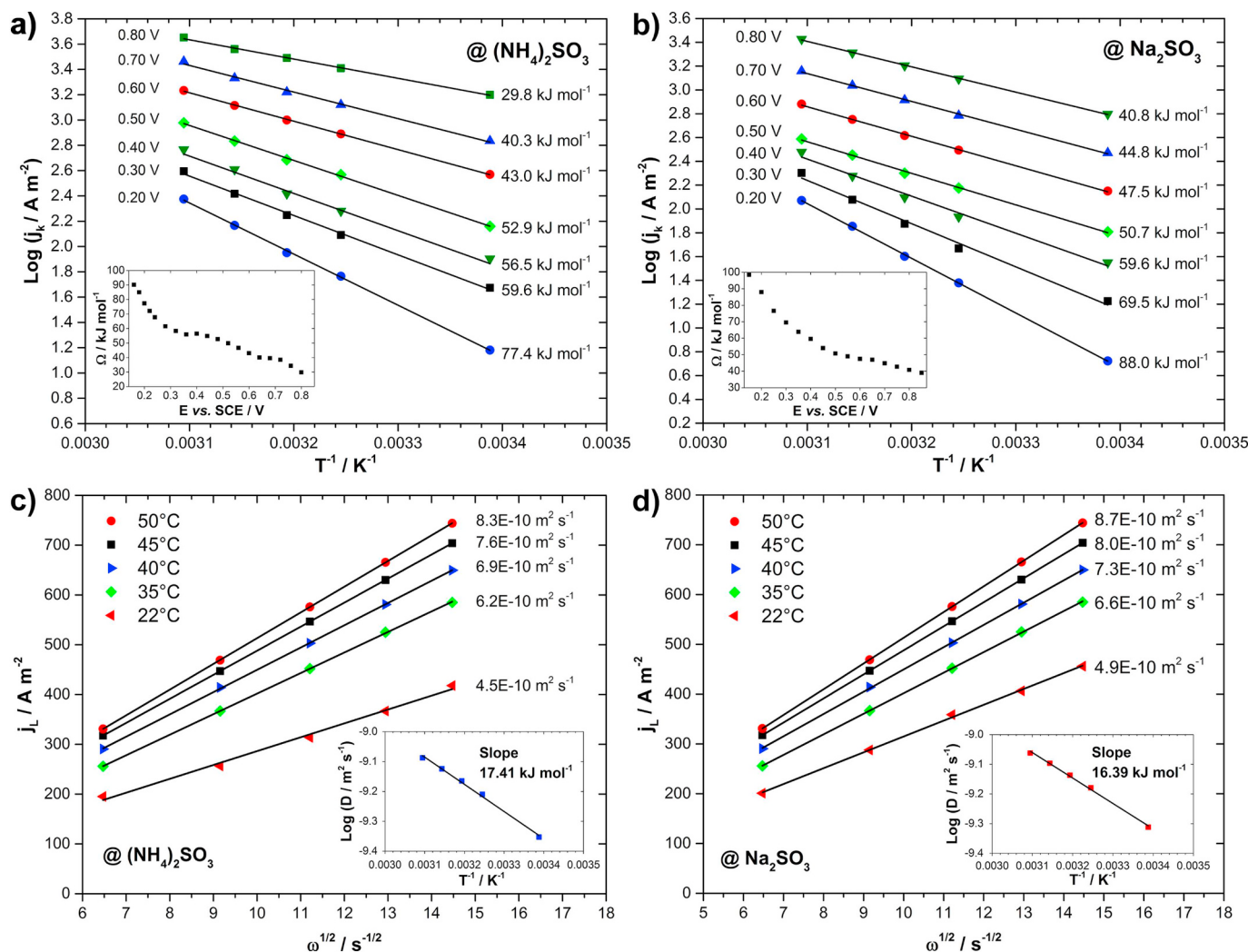
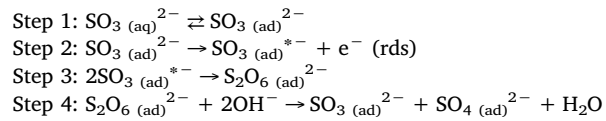


Fig. 6. Plots of $\log(j_k)$ as a function of T^{-1} for different potentials (above) and j_L against $\omega^{1/2}$ for different rotation rates (below) at different temperatures.



At high potentials sulfite desorption occurs, according to β values of 0.22 [12,13]. Since the values in Table 1 and Table 3 are comparable, it is evident that higher temperatures and potentials above 0.30 V promote desorption. Hence, we propose a mechanism analogous to that described above in which sulfite is directly oxidized on the surface at high potentials.

The presence of dithionite, especially for ammonium sulfite, is considered in the light of the following facts:

- The literature claims that the highest yield of dithionite occurs at around pH 7 [34].
- A multistep pathway is presumed since large Tafel slopes (Table 1) are characteristic of sluggish reactions and depletion of reaction sites [8]. The shift in the intercept of Eq. (3) (Fig. 2a inset) supports this.

Special attention must be paid to ammonium sulfite at high potentials. Since this shows erratic behavior, a clear mechanism cannot be defined and further studies are required.

A rate expression for electrooxidation is proposed, considering Step 2 as the rds:

$$j = \frac{nFk_s^0 \theta_{\text{SO}_3^{(\text{ad})2-}} \exp\left[-\frac{\beta nF(E - E^0)}{RT}\right]}{1 + \frac{k_s^0 \exp\left[-\frac{\beta nF(E - E^0)}{RT}\right]}{k_D}} \quad (12)$$

where E^0 is the standard electrode potential, k_D is the mass transfer coefficient, k_s^0 is the heterogeneous rate constant, and $\theta_{\text{SO}_3^{(\text{ad})2-}}$ is the surface coverage of sulfite. Eq. (12) was validated using a multistep approach described in the supplementary data (pp. S11–S13).

4. Conclusions

Pd/C exhibits good catalytic activity for electrooxidation of sulfite in near-neutral pH electrolytes, when sodium sulfite displays higher current densities. Kinetics results suggest that sulfite electrooxidation occurs through an adsorption mechanism at low potentials, while sulfite is directly oxidized on the electrode surface at high potentials. The performance of Pd is comparable to Pt, especially at pH 8.5. Hence, Pd could be used for sulfite electrooxidation at near-neutral or slightly alkaline conditions, offering a useful approach for ammonia-based FGD.

Acknowledgements

The authors acknowledge the financial support received from the Sector Fund CONACYT-SENER-ENERGY-SUSTAINABILITY 207450 within Strategic Project No. 10, entitled: "Solar Fuels & Industrial Processes", by which it was possible to carry out experimental work.

Appendix A. Supplementary data

Supplementary data to this article can be found online at <https://doi.org/10.1016/j.elecom.2019.106481>.

References

- [1] M.Z. Jacobson, Energy Environ. Sci. 2 (2009) 148–173.
- [2] WHO, Air Quality Guidelines for Particulate Matter, Ozone, Nitrogen Dioxide and Sulfur Dioxide, World Health Organization, Geneva, 2006.
- [3] S. Yan, G. Wu, Sci. Rep. 7 (2017) 46216.
- [4] D. Flagiello, A. Erto, A. Lancia, F. Di Natale, Fuel 214 (2018) 254–263.
- [5] J. Wang, P. Yang, Renew. Sust. Energ. Rev. 82 (2018) 1969–1978.
- [6] Y. Li, K. Shang, N. Lu, J. Li, Y. Wu, J. Phys. Conf. Ser. 418 (2013) 012130.
- [7] J. Han, H. Cheng, L. Zhang, H. Fu, J. Chen, Chem. Eng. J. 335 (2018) 231–235.
- [8] J.A. O'Brien, J.T. Hinkley, S.W. Donne, S.E. Lindquist, Electrochim. Acta 55 (2010) 573–591.
- [9] C. Huang, Sol. Energy 91 (2013) 394–401.
- [10] M. Bouroushan, *Electrochemistry of Metal Chalcogenides*, Springer-Verlag Berlin, Heidelberg Berlin, 2010.
- [11] R. Arce, M.J. Aguirre, J. Romero, Int. J. Electrochem. Sci. 9 (2014) 7916–7924.
- [12] E. Skavås, T. Hemmingsen, Electrochim. Acta 52 (2007) 3510–3517.
- [13] J. Lu, D.B. Dreisinger, W.C. Cooper, J. Appl. Electrochem. 29 (1999) 1161–1170.
- [14] A.G. Zelinsky, Electrochim. Acta 188 (2016) 727–733.
- [15] Y.V. Tolmachev, D.A. Scherson, Electrochim. Acta 49 (2004) 1315–1319.
- [16] S. Díaz-Abad, M. Millán, M.A. Rodrigo, J. Lobato, Catalysts 9 (2019) 63.
- [17] R. Li, Z. Wei, T. Huang, A. Yu, Electrochim. Acta 56 (2011) 6860–6865.
- [18] M. Shao, J. Power Sources 196 (2011) 2433–2444.
- [19] A.G. Zelinsky, B.Y. Pirogov, Electrochim. Acta 231 (2017) 371–378.
- [20] J.G. Bell, M. Dao, J. Wang, J. Electroanal. Chem. 816 (2018) 1–6.
- [21] Y. Garsany, I.L. Singer, K.E. Swider-Lyons, J. Electroanal. Chem. 662 (2011) 396–406.
- [22] Y. Garsany, O.A. Baturina, K.E. Swider-Lyons, S.S. Kocha, Anal. Chem. 82 (2010) 6321–6328.
- [23] Z.X. Liang, T.S. Zhao, J.B. Xu, L.D. Zhu, Electrochim. Acta 54 (2009) 2203–2208.
- [24] R.M. Modibedi, T. Mehlo, K.I. Ozoemena, M.K. Mathe, Int. J. Hydrog. Energy 40 (2015) 15605–15612.
- [25] M. Grdeň, M. Łukaszewski, G. Jerkiewicz, A. Czerwiński, Electrochim. Acta 53 (2008) 7583–7598.
- [26] H.R. Colón-Mercado, D.T. Hobbs, Electrochim. Commun. 9 (2007) 2649–2653.
- [27] A. Bard, L. Faulkner, *Electrochemical Methods: Fundamentals and Applications*, Second ed., Wiley, New York, 2000.
- [28] E. Skavas, M. Adriaens, T. Hemmingsen, Int. J. Electrochem. Sci. 1 (2006) 414–424.
- [29] V.S. Protsenko, F.I. Danilov, J. Electroanal. Chem. 651 (2011) 105–110.
- [30] P. Gründler, A. Kirbs, L. Dunsch, ChemPhysChem 10 (2009) 1722–1746.
- [31] T. Hunger, F. Lapicque, Electrochim. Acta 36 (1991) 1073–1082.
- [32] A.G. Zelinsky, Electrochim. Acta 154 (2015) 315–320.
- [33] L.A. Diaz, G.G. Botte, Electrochim. Acta 179 (2015) 519–528.
- [34] S. Glasstone, A. Hickling, J. Chem. Soc. (1933) 829–836.